

Empowering the Smart Grid: Can Redox Batteries be Matched to Renewable Energy Systems for Energy Storage?

Jonathan E. Halls,^{*1†} Amanda Hawthornthwaite,^{1‡} Russell J. Hepworth,^{1‡}

Noel A. Roberts,¹ Kevin J. Wright,¹ Yan Zhou,¹ Stephen J. Haswell,¹

Stephanie K. Haywood,² Stephen M. Kelly,¹ Nathan S. Lawrence,³ Jay D. Wadhawan^{*1}

¹*Department of Chemistry, The University of Hull,*

Cottingham Road, Kingston-upon-Hull HU6 7RX, United Kingdom.

²*Centre for Adaptive Science & Sustainability, The University of Hull,*

Cottingham Road, Kingston-upon-Hull HU6 7RX, United Kingdom.

³*Schlumberger Cambridge Research, Ltd., High Cross,*

Madingley Road, Cambridge CB3 0EL, United Kingdom.

[†]Present address: Department of Chemistry, The University of Bath, Claverton Down, Bath BA2 7AY, United Kingdom.

[‡]Present address: Reckitt Benckiser Health Care (UK), Ltd., Dansom Lane, Kingston-upon-Hull HU8 7LN, United Kingdom.

[‡]Present address: Severn Trent Water, Plc., Analytical Services Division, Sheffield, United Kingdom.

*Corresponding authors

E.mail: j.e.halls@bath.ac.uk (JEH); j.wadhawan@hull.ac.uk (JDW)

Electronic Supporting Information

Contents

S1	<i>Electrical Characteristics of an Ideal Battery</i>	S2
S2	<i>Discussion of the Battery Chemistry</i>	S3
S3	<i>Calculation of Corrosive Mixed-Potentials at Open Circuit</i>	S4
S4	<i>Details of the Pentadiagonal Matrix Algorithm Employed</i>	S6
S5	<i>Computation of Electrode Potentials during Charge/Discharge</i>	S8
S6	<i>Iterative Strategy for Capacitive Current</i>	S10
S7	<i>Computing</i>	S11
S8	<i>References</i>	S12

S1: Electrical Characteristics of an Ideal Battery

For an ideal cell, charged to an arbitrary SOC, to afford a terminal potential difference at open circuit of V_{oc} , the *maximum energy deliverable* is $V_{oc}Q_0$. The constant current discharge of this battery, of internal resistance R_s , over an external resistance, R_i , affords, by Kirchhoff's laws, a terminal potential difference, V , of:

$$V = iR_i = V_{oc} - iR_s \quad (S1.1)$$

Clearly, under open circuit conditions, when $i \rightarrow 0, V \rightarrow V_{oc}$. At short circuit, $V = 0$, allowing a maximum current, i_{sc} , to flow:

$$i_{sc} = \frac{V_{oc}}{R_s} \quad (S1.2)$$

Now, the electrical power delivered across the load is

$$p = iV = i(V_{oc} - iR_s) = iV_{oc} - i^2 \frac{V_{oc}}{i_{sc}} \quad (S1.3)$$

so that the current flowing in terms of the power delivered is:

$$i = \frac{i_{sc}}{2} \pm \sqrt{\frac{i_{sc}^2}{4} - p \frac{i_{sc}}{V_{oc}}} \quad (S1.4)$$

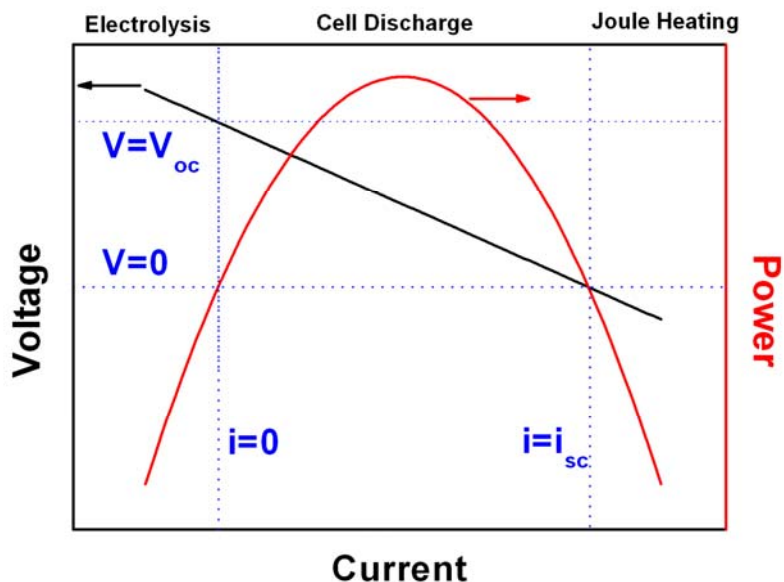


Figure S1.1: Characteristics of an ideal battery, identifying the electrolytic, galvanic and supergalvanic regions from left-to-right.

Thus, as $p \rightarrow 0$, $i \rightarrow 0$ (open circuit conditions, corresponding to $R_i \rightarrow \infty$) or $i \rightarrow i_{sc}$ (short circuit conditions, corresponding to $R_i \rightarrow 0$) – in these two limits, no electrical power is produced. The maximum power that can be delivered by the ideal battery can be determined from,

$$\frac{dp}{dV} = i_{sc} - 2i_{sc} \frac{V}{V_{oc}} = 0 \quad (\text{S1.5})$$

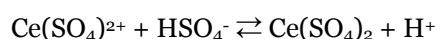
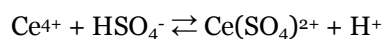
furnishing a current at the power point of $i_{mp} = \frac{1}{2}i_{sc}$ at an associated voltage $V_{mp} = \frac{1}{2}V_{oc}$, indicating

that the maximum power that can be drawn from the ideal battery is $p_{max} = \frac{1}{4}i_{sc}V_{oc}$, as indicated in

Figure S1.1. Also indicated in this figure are the electrolytic ($i < 0$) and supergalvanic ($i_{sc} > 0$) regimes, where electrical power has to be *supplied* to the galvanic cell for charging ($p < 0$, $i < 0$, $V > V_{oc}$), or for Joule heating ($p < 0$, $i > i_{sc}$, $V < 0$).

S2: Discussion of the Battery Chemistry

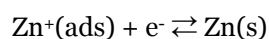
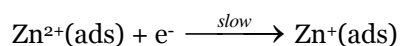
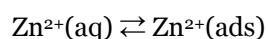
It is well-known,^{S1} in acidic aqueous solutions, the thermodynamic and kinetic oxidising ability of cerium(IV) depends on the nature of the acid counter ion: in H_2SO_4 , the following complexation reactions are thought to occur.^{S2a}



with the last anionic cerium(IV) form predominating at high H_2SO_4 concentrations, thereby suppressing hydrolysis of Ce^{4+} . Accordingly, we suppose that the formal electrode potential for the cerium(III)/cerium(IV) half-cell within methanesulfonic acid is the same as in sulfuric acid. Although the value of the standard heterogeneous rate constant (k_s) for the reduction of Ce^{4+} varies in the literature^{S2b} from $5.3 \times 10^{-5} - 13.0 \times 10^{-4} \text{ cm s}^{-1}$, the electrode reaction is sluggish on most electrodes, and occurs with a transfer coefficient (α) in the range 0.1 – 0.5; Randle and Kuhn^{S2b} have used such data to provide evidence to suggest the electrode reaction involves the sulfato-complexes forms in sulfuric acid. Nevertheless, we shall consider only the basic electron transfer reaction, using literature-averaged values for k_s and α .

Likewise, the reduction of zinc is considered to occur as a single two-electron process,^{S1} even though it is known^{S3a} that zinc reduction (at least on mercury) occurs in a CE type process, involving the adsorption of zinc ions. Nevertheless, the single step process is also kinetically slow (the standard rate constant and symmetry factor given above are also averages taken from the literature^{S3a,b,S4e}), with nucleation (at least on carbon) thought to proceed through an instantaneous (rather than progressive) mechanism,^{S4c} *viz.* the number density of nucleation centres equals the number of active sites - a time-independent constant. We assume that voltage ripple (AC variation superimposed on DC) has no effect on zinc plating uniformity,^{S3c} and likewise, as mentioned earlier, suppose that the electrolyte contains additives to suppress dendrite formation during zinc plating. Moreover, we assume that the plating of zinc onto the electrode during charge does not alter the cell thickness, as this would otherwise require a dynamic, not static, spatial grid to be deployed. This is a reasonable assumption since approximately $\frac{|A|t_s}{F}$ mol of zinc are deposited, corresponding to ~4000 monolayers, resulting in uniform deposits that are ~520 nm thick (assuming^{S5} an atomic radius of zinc of 133.2 pm), which is *ca.* 1% of the thinnest cell depth considered in this work, *vide infra*).

The less-than-unity value of the transfer coefficient for zinc ion reduction (taken to be 0.4 in this work) is consistent with a near-symmetric barrier of a single step two-electron process ($2\alpha_2 = 0.8 \approx 1$), rather than the adsorbed single charge species mechanism that is thought to occur in neutral and non-complexing solutions:^{S3b}



The assumption that the electrolyte contains corrosion inhibitors to suppress the hydrogen evolution reaction (*vide supra*) is reasonable: the standard exchange current density for hydrogen oxidation on zinc at 298 K is reported^{S6} as being 10^{-11} A cm⁻².

S3: Calculation of Corrosive Mixed-Potentials at Open Circuit

To account for mixed-potentials due to corrosion at open-circuit when no current flows between the two electrodes, the net corrosion current has to be zero; provided corrosion occurs *uniformly* over the

zinc electrode, the total reduction rate must match the total rate of oxidation, at every point on the surface, *viz.*,

$$i_{Ce^{4+} \rightarrow Ce^{3+}}^{corr} = 2i_{Zn \rightarrow Zn^{2+}}^{corr} \quad (S3.1)$$

in which the factor of two for the zinc dissolution current merely reflects the reaction stoichiometry.

Hence, under a Butler-Volmer formalism,^{S7}

$$k_{s_3} (c_{Ce^{4+}})_{x=\ell} e^{\alpha_3 \frac{F}{RT} E_{cell}^{0'}} e^{-\alpha_3 \xi_2} + 2k_{s_2} (c_{Zn^{2+}})_{x=\ell} e^{-2\alpha_2 \xi_2} = k_{s_3} (c_{Ce^{3+}})_{x=\ell} e^{(\alpha_3-1) \frac{F}{RT} E_{cell}^{0'}} e^{(1-\alpha_3) \xi_2} + 2k_{s_2} c_s e^{2(1-\alpha_2) \xi_2} \quad (S3.2)$$

where k_{s_3} is the standard heterogeneous rate constant for Ce^{4+} reduction on zinc, with α_3 the

associated symmetry factor and denote the reduced potential $\xi_2 = \frac{F}{RT} (E_{LHS} - E_{Zn|Zn^{2+}}^{0'})$. For the

case when $\alpha_3 = 2\alpha_2 = 1$, the above can be solved to afford the following expression for the corrosion potential.

$$E_{LHS} = E_{Zn|Zn^{2+}}^{0'} + \frac{RT}{F} \ln \left\{ \frac{-k_{s_3} (c_{Ce^{3+}})_{x=\ell} + \sqrt{k_{s_3}^2 (c_{Ce^{3+}})_{x=\ell}^2 + 8k_{s_2} c_s \left\{ 2k_{s_2} (c_{Zn^{2+}})_{x=\ell} + k_{s_3} (c_{Ce^{4+}})_{x=\ell} e^{\frac{F}{RT} E_{cell}^{0'}} \right\}}}{4k_{s_2} c_s} \right\} \quad (S3.3)$$

Satisfyingly, the above reduces to the Nernst expression in the absence of cerium-induced zinc corrosion, *viz.* when $k_{s_3} = 0$. Thus, for the general case of $\alpha_3 \neq 2\alpha_2 \neq 1$, the above was used as a first approximation in a Newton-Raphson iterative solution (dummy variable ζ), with subsequent estimates of the corrosion potential determined through the relation,

$$\chi_\zeta = \chi_{\zeta-1} - \frac{k_{s_3} (c_{Ce^{4+}})_{x=\ell} e^{\alpha_3 \frac{F}{RT} E_{cell}^{0'}} - k_{s_3} (c_{Ce^{3+}})_{x=\ell} e^{(\alpha_3-1) \frac{F}{RT} E_{cell}^{0'}} \chi_{\zeta-1} - 2k_{s_2} c_s \chi_{\zeta-1}^{\{\alpha_3+2(1-\alpha_2)\}} + 2k_{s_2} (c_{Zn^{2+}})_{x=\ell} \chi_{\zeta-1}^{\{\alpha_3-2\alpha_2\}}}{-k_{s_3} (c_{Ce^{3+}})_{x=\ell} e^{(\alpha_3-1) \frac{F}{RT} E_{cell}^{0'}} - 2k_{s_2} c_s \{\alpha_3 + 2(1-\alpha_2)\} \chi_{\zeta-1}^{\alpha_3+1-2\alpha_2} + 2k_{s_2} (c_{Zn^{2+}})_{x=\ell} (\alpha_3 - 2\alpha_2) \chi_{\zeta-1}^{\{\alpha_3-2\alpha_2-1\}}} \quad (S3.4)$$

where $\chi = e^{\xi_2}$. Typically, 29 iterations were required for non-zero values of k_{s_3} to achieve convergence to within the required threshold (10^{-10} in χ).

S4: Details of the Pentadiagonal Matrix Algorithm Employed

We follow the method outlined in reference S8, and provide corrected expressions. We note that this approach is computationally more efficient than that employed in our earlier work.^{S9}

We consider the solution of $N \times N$ simultaneous equations, described by the matrix equation,

$$[T]\{u\} = \{m\} \quad (\text{S4.1})$$

where $[T]$ is an $N \times N$ pentadiagonal matrix where all coefficients are known, $\{u\}$ is a vector of N unknowns, and $\{m\}$ is a vector of N known values. Proceeding *via* LU decomposition of $[T]$ yields

$$[T] = [T_L][T_U] \quad (\text{S4.2})$$

We next seek a vector $\{f\}$, such that

$$[T_L]\{f\} = \{m\} \quad (\text{S4.3})$$

so that,

$$[T_U]\{u\} = \{f\} \quad (\text{S4.4})$$

and, therefore,

$$[T_U]\{u\} = [T_L]^{-1}\{m\} \quad (\text{S4.5})$$

since

$$\{f\} = [T_L]^{-1}\{m\} \quad (\text{S4.6})$$

Thus,

$$[T_L][T_U]\{u\} = \{m\} \quad (\text{S4.7})$$

as required.

Noting that $1 \leq j \leq N$ and defining,

$$[T] = \begin{bmatrix} a_1 & b_1 & c_1 & 0 & & & & & 0 \\ d_2 & a_2 & b_2 & c_2 & 0 & & & & 0 \\ e_3 & d_3 & a_3 & b_3 & c_3 & 0 & & & 0 \\ & \searrow & & & & \searrow & & & \\ 0 & 0 & e_j & d_j & a_j & b_j & c_j & 0 & 0 \\ & & & \searrow & & & \searrow & & \\ 0 & & & 0 & e_{N-2} & d_{N-2} & a_{N-2} & b_{N-2} & c_{N-2} \\ 0 & & & & 0 & e_{N-1} & d_{N-1} & a_{N-1} & b_{N-1} \\ 0 & & & & & 0 & e_N & d_N & a_N \end{bmatrix} \quad (\text{S4.8})$$

$$[T_L] = \begin{bmatrix} 1 & 0 & & & & & & & 0 \\ z_2 & 1 & 0 & & & & & & 0 \\ \frac{e_3}{x_1} & z_3 & 1 & 0 & & & & & 0 \\ & \searrow & & \searrow & & & & & \\ 0 & \frac{e_j}{x_{j-2}} & z_j & 1 & 0 & & & & 0 \\ & & \searrow & & \searrow & & & & \\ 0 & & 0 & \frac{e_{N-2}}{x_{N-4}} & z_{N-2} & 1 & 0 & 0 & 0 \\ 0 & & & 0 & \frac{e_{N-1}}{x_{N-3}} & z_{N-1} & 1 & 0 & 0 \\ 0 & & & & 0 & \frac{e_N}{x_{N-2}} & z_N & 1 & 0 \end{bmatrix} \quad (\text{S4.9})$$

and

$$[T_U] = \begin{bmatrix} x_1 & y_1 & c_1 & 0 & & & & & 0 \\ 0 & x_2 & y_2 & c_2 & 0 & & & & 0 \\ 0 & 0 & x_3 & y_3 & c_3 & 0 & & & 0 \\ & & & \searrow & & \searrow & & & \\ 0 & & & 0 & x_j & y_j & c_j & 0 & 0 \\ & & & & & \searrow & \searrow & & \\ 0 & & & & 0 & x_{N-2} & y_{N-2} & c_{N-2} & \\ 0 & & & & & 0 & x_{N-1} & y_{N-1} & \\ 0 & & & & & & 0 & x_N & \end{bmatrix} \quad (\text{S4.10})$$

$$\{u\} = \begin{Bmatrix} u_1 \\ u_2 \\ u_3 \\ \vdots \\ u_j \\ \vdots \\ u_{N-2} \\ u_{N-1} \\ u_N \end{Bmatrix} \text{ and } \{m\} = \begin{Bmatrix} m_1 \\ m_2 \\ m_3 \\ \vdots \\ m_j \\ \vdots \\ m_{N-2} \\ m_{N-1} \\ m_N \end{Bmatrix} \quad (\text{S4.11})$$

allows the following variables to be defined.

$$x_1 = a_1; x_2 = a_2 - z_2 y_1; x_j = a_j - z_j y_{j-1} - \frac{e_j}{x_{j-2}} c_{j-2}; y_1 = b_1; y_j = b_j - z_j c_{j-1};$$

$$z_2 = \frac{d_2}{x_1}; z_i = \frac{d_i - \frac{e_i}{x_{i-2}} y_{i-2}}{x_{i-1}} \quad (\text{S4.12})$$

It thus follows, from forward recursion that,

$$f_1 = m_1; f_2 = m_2 - z_2 f_1; f_j = m_j - z_j f_{j-1} - \frac{e_j}{x_{j-2}} f_{j-2} \quad (\text{S4.13})$$

and therefore, the required solution may be found through backward recursion,

$$u_N = \frac{f_N}{x_N}; u_{N-1} = \frac{f_{N-1} - y_{N-1} u_N}{x_{N-1}}; u_j = \frac{f_j - y_j u_{j+1} - c_j u_{j+2}}{x_j} \quad (\text{S4.14})$$

S5: Computation of Electrode Potentials during Charge/Discharge

Thus, under current-controlled (galvanostatic) discharge, the surface concentrations of all species may be ascertained through the following finite difference relationships of the Neumann boundary conditions at the electrode surfaces, where we use square brackets to denote concentrations normalised by the speciation-independent total concentration of cerium ions, with surface concentrations reduced through normalisation with the maximum possible surface coverage (Γ_T).

$$\left[Ce^{3+} \right]_0^t = \left[Ce^{3+} \right]_1^t + \frac{i_f \Delta x}{FSD_{Ce^{3+}} (c_{Ce^{3+}}^0 + c_{Ce^{4+}}^0)} \quad (\text{S5.1})$$

$$[Ce^{4+}]_0^t = [Ce^{4+}]_1^t - \frac{i_f \Delta x}{FSD_{Ce^{4+}} (c_{Ce^{3+}}^0 + c_{Ce^{4+}}^0)} \quad (S5.2)$$

$$[Zn^{2+}]_0^t = [Zn^{2+}]_1^t \quad (S5.3)$$

$$[Zn^{2+}]_\ell^t = [Zn^{2+}]_{\ell-1}^t + \frac{i_f \Delta x}{2FSD_{Zn^{2+}} (c_{Ce^{3+}}^0 + c_{Ce^{4+}}^0)} - \frac{D_{Ce^{4+}}}{2D_{Zn^{2+}}} \left\{ [Ce^{4+}]_\ell^t - [Ce^{4+}]_{\ell-1}^t \right\} \quad (S5.4)$$

$$[\Gamma_{Zn}]^t = [\Gamma_{Zn}]^{t-1} - \frac{D_{Zn^{2+}} \Delta t (c_{Ce^{3+}}^0 + c_{Ce^{4+}}^0)}{\Delta x \Gamma_T} \left\{ [Zn^{2+}]_\ell^t - [Zn^{2+}]_{\ell-1}^t \right\} \quad (S5.5)$$

$$[Ce^{4+}]_\ell^t = \left\{ \frac{\frac{D_{Ce^{4+}}}{\Delta x} - k_{s_3} e^{(1-\alpha_3)\xi_3} \frac{D_{Ce^{4+}}}{D_{Ce^{3+}}}}{\frac{D_{Ce^{4+}}}{\Delta x} - k_{s_3} e^{-\alpha_3 \xi_3} - k_{s_3} e^{(1-\alpha_3)\xi_3} \frac{D_{Ce^{4+}}}{D_{Ce^{3+}}}} \right\} [Ce^{4+}]_{\ell-1}^t - \left\{ \frac{k_{s_3} e^{(1-\alpha_3)\xi_3}}{\frac{D_{Ce^{4+}}}{\Delta x} - k_{s_3} e^{-\alpha_3 \xi_3} - k_{s_3} e^{(1-\alpha_3)\xi_3} \frac{D_{Ce^{4+}}}{D_{Ce^{3+}}}} \right\} [Ce^{3+}]_{\ell-1}^t \quad (S5.6)$$

$$[Ce^{3+}]_\ell^t = \left\{ 1 + \frac{\frac{D_{Ce^{4+}}}{\Delta x} - k_{s_3} e^{(1-\alpha_3)\xi_3} \frac{D_{Ce^{4+}}}{D_{Ce^{3+}}}}{\frac{D_{Ce^{4+}}}{\Delta x} - k_{s_3} e^{-\alpha_3 \xi_3} - k_{s_3} e^{(1-\alpha_3)\xi_3} \frac{D_{Ce^{4+}}}{D_{Ce^{3+}}}} \right\} [Ce^{3+}]_{\ell-1}^t - \frac{D_{Ce^{4+}}}{D_{Ce^{3+}}} \left\{ 1 - \frac{\frac{D_{Ce^{4+}}}{\Delta x} - k_{s_3} e^{(1-\alpha_3)\xi_3} \frac{D_{Ce^{4+}}}{D_{Ce^{3+}}}}{\frac{D_{Ce^{4+}}}{\Delta x} - k_{s_3} e^{-\alpha_3 \xi_3} - k_{s_3} e^{(1-\alpha_3)\xi_3} \frac{D_{Ce^{4+}}}{D_{Ce^{3+}}}} \right\} [Ce^{4+}]_{\ell-1}^t \quad (S5.7)$$

These calculated values can then be employed to determine the potentials at each electrode. For the case of the right-hand electrode, this was undertaken through Newton-Raphson iteration (dummy index q),

$$\mathcal{G}_q = \mathcal{G}_{q-1} - \frac{\left(\frac{i_f}{k_s FS (c_A^0 + c_B^0)} \right) \mathcal{G}_{q-1}^\alpha + [Ce^{3+}]_0^t \mathcal{G}_{q-1} - [Ce^{4+}]_0^t}{\alpha \left(\frac{i_f}{k_s FS (c_A^0 + c_B^0)} \right) \mathcal{G}_{q-1}^{\alpha-1} + [Ce^{3+}]_0^t} \quad (S5.8)$$

where $\mathcal{G} = \exp(\xi)$, and to a threshold of 10^{-10} in \mathcal{G} , employing, as a first approximation, the

potential obtained when $\alpha = \frac{1}{2}$, viz.,

$$E_{Ce^{3+}|Ce^{4+}} = E_{Ce^{3+}|Ce^{4+}}^{0'} + \frac{2RT}{F} \ln \left[\frac{1}{2 [Ce^{3+}]_0^t k_s FS (c_{Ce^{3+}}^0 + c_{Ce^{4+}}^0)} + \sqrt{\left\{ \frac{i_f}{k_s FS (c_{Ce^{3+}}^0 + c_{Ce^{4+}}^0)} \right\}^2 + 4 [Ce^{3+}]_0^t [Ce^{4+}]_0^t} \right]$$

$$(S5.9)$$

Typically three iterations were required for convergence of the electrode potential. The mixed-flux boundary condition for the left-hand electrode causes a slightly more intricate calculation to take place, again through Newton-Raphson iteration (dummy variable ζ),

$$\chi_{\zeta} = \chi_{\zeta-1} - \frac{\left(\frac{i_f}{FS(c_{Ce^{3+}}^0 + c_{Ce^{4+}}^0)} \right) \chi_{\zeta-1}^{\alpha_3} - 2k_{s_2} [Zn^{2+}]_{\ell}^t \chi_{\zeta-1}^{(\alpha_3-2\alpha_2)} + 2k_{s_2} \left\{ \frac{c_s}{(c_{Ce^{3+}}^0 + c_{Ce^{4+}}^0)} \right\} \chi_{\zeta-1}^{\{\alpha_3+2(1-\alpha_2)\}} + k_{s_3} [Ce^{3+}]_{\ell}^t e^{\frac{(\alpha_3-1)F}{RT} E_{cell}^0} \chi_{\zeta-1} - k_{s_3} [Ce^{4+}]_{\ell}^t e^{\frac{\alpha_3 F}{RT} E_{cell}^0}}{\left(\frac{i_f}{FS(c_{Ce^{3+}}^0 + c_{Ce^{4+}}^0)} \right) \alpha_3 \chi_{\zeta-1}^{(\alpha_3-1)} - 2k_{s_2} [Zn^{2+}]_{\ell}^t (\alpha_3 - 2\alpha_2) \chi_{\zeta-1}^{(\alpha_3-2\alpha_2-1)} + 2k_{s_2} \left\{ \frac{c_s}{(c_{Ce^{3+}}^0 + c_{Ce^{4+}}^0)} \right\} (2-2\alpha_2 + \alpha_3) \chi_{\zeta-1}^{(1-2\alpha_2+\alpha_3)} + k_{s_3} [Ce^{3+}]_{\ell}^t e^{\frac{(\alpha_3-1)F}{RT} E_{cell}^0}}$$

$$(S5.10)$$

employing, for the first approximation, the solution obtained for the case of $\alpha_3 = 2\alpha_2 = 1$, viz.

$$\chi = \frac{(c_{Ce^{3+}}^0 + c_{Ce^{4+}}^0)}{4k_{s_2} c_s} - \left\{ k_{s_3} [Ce^{3+}]_{\ell}^t + \frac{i_f}{FS(c_{Ce^{3+}}^0 + c_{Ce^{4+}}^0)} \right\} + \sqrt{\left\{ k_{s_3} [Ce^{3+}]_{\ell}^t + \frac{i_f}{FS(c_{Ce^{3+}}^0 + c_{Ce^{4+}}^0)} \right\}^2 + 8k_{s_2} c_s \left\{ k_{s_3} [Ce^{4+}]_{\ell}^t e^{\frac{F}{RT} E_{cell}^0} + 2k_{s_2} [Zn^{2+}]_{\ell}^t \right\}}$$

$$(S5.11)$$

A maximum of 28 iterations were required for the potentials to be converged to within the required threshold (10^{-10} in χ). Note that in the case when zinc corrosion/depletion is such that $\Gamma_{Zn} = 0$, all terms involving c_s are set to zero, so that a first approximation to the electrode potential is:

$$\xi_2 = \ln \left(\frac{2k_{s_2} + k_{s_3} [Ce^{4+}]_{\ell}^t e^{\frac{F}{RT} E_{cell}^0}}{k_{s_3} [Ce^{3+}]_{\ell}^t + \frac{i}{FS(c_{Ce^{3+}}^0 + c_{Ce^{4+}}^0)}} \right)$$

$$(S5.12)$$

Thus, in the absence of effects due to double layer charging or Ohmic drop, the cell voltage is:

$$E_{cell} = E_{Ce^{3+}|Ce^{4+}} - E_{Zn|Zn^{2+}}$$

$$(S5.13)$$

S6: Iterative Strategy for Capacitive Current

We adopted the following iterative strategy to compute the non-Faradaic component. Initially, the capacitive current was assumed to be zero, so that the cell voltage could be determined as above, albeit with Ohmic losses accounted through: $V = E_{cell} - iR_s$. Note that this causes the cell voltage to be increased compared with the case of no Ohmic drop (charging currents are negative), and decreased under discharge. This allows for the first approximation to the capacitive contribution, using,

$$|i_{cap}| = \left| \frac{d}{dt} (SQ_{cap}) \right| = S \left| \frac{dQ_{cap}}{dt} \right| + Q_{cap} \left| \frac{dS}{dt} \right| = C_{dl} S \left| \frac{dE_{cell}}{dt} \right| = \frac{1}{5} \left| \frac{dE_{cell}}{dt} \right| \quad (S6.1)$$

assuming that the electrode contact area with the electrolyte is constant (*viz.* no gas produced/phase change/dendrite formation), and in which Q_{cap} is the charge density of the electrode | electrolyte interface. Note that the capacitive current is dependent on the rate at which the voltage across the *Warburg impedance* varies, and so does not include the Ohmic correction, as is evident from the equivalent circuit illustrated in Figure 1 of the main text. The *charging* of the capacitor *diminishes* the Faradaic current, reducing the extent of electrolysis,

$$i_f^{charge} = i^{charge} + |i_{cap}| \quad (S6.2)$$

where i^{charge} is negative. Under discharge, since the temporal change in the cell voltage *generates* a capacitive current to flow, capacitive discharge also *decreases* the Faradaic current that is allowed to flow:

$$i_f^{discharge} = i^{discharge} - |i_{cap}| \quad (S6.3)$$

These first estimates were then employed to recalculate both i_f and V iteratively, to an absolute error of $<1.0 \mu\text{A}$ in $|i_{cap}|$. A maximum of three iterations were found to be necessary.

S7: Computing

Dense spatio-temporal grids were found to be required (typically 50000 nodes in time and 20000 nodes in space) to ensure sufficient numerical convergence of the resulting concentration profiles; the use of $\Delta t \gg R_s C_{dl}$ assisted in damping oscillatory instabilities under short times due to the small cell time constants. Furthermore, to avoid the cell cutting out to open circuit due to complete electrolysis, except for the case of the week-long solar charging simulation, all data reported herein were obtained under the condition that the concentrations of all species (including the surface concentration of zinc) were greater than zero (a necessary constraint for finite difference simulations of galvanic cells^{S10}) with $\frac{dV}{dt} \leq 0$ under discharge; this constraint is tantamount to the “cut-off” voltage used in experimental battery testing. Simulations were undertaken through program encoding in GNU FORTRAN with double precision variables using the freely available g77 compiler, and were executed

on an Intel Pentium processor (2.4 GHz; 1.98 GB RAM). Single charge-discharge experiments typically were found to cost a maximum of *ca.* 250 s in CPU time.

S8: References

- S1. See, for example, A. J. Bard, R. Parsons, J. Jordan (eds.), *Standard Potentials in Aqueous Solution*, Marcel Dekker, New York, 1985.
- S2. (a) A. K. Das, *Co-ord. Chem. Rev.*, 2001, **213**, 307; (b) T. H. Randle, A. T. Kuhn, *J. Chem. Soc., Faraday Trans. 1*, 1983, **79**, 1741; (c) P. Trinidad, C. Ponce de León, F. C. Walsh, *J. Environ. Management*, 2008, **88**, 1417.
- S3. (a) I. S. El-Hallag, *J. Chil. Chem. Soc.*, 2010, **55**, 374; (b) L. Gaiser, K. E. Heusler, *Electrochim. Acta*, 1970, **15**, 161; (c) B. Stein, *Metal Finishing*, 1985, 100.
- S4. (a) P. K. Leung, C. Ponce de León, C. T. J. Low, A. A. Shah, F. C. Walsh, *J. Power Sources*, 2011, **196**, 5174; (b) P. K. Leung, C. Ponce de León, C. T. J. Low, F. C. Walsh, *Electrochim. Acta*, 2011, **56**, 2145; (c) G. Nikiforidis, L. Berlouis, D. Hall, D. Hodgson, *J. Power Sources*, 2012, **206**, 497; (d) P. K. Leung, C. Ponce de León, F. C. Walsh, *Electrochem. Commun.*, 2011, **13**, 770; (e) P. K. Leung, C. Ponce de León, C. T. J. Low, F. C. Walsh, *Electrochim. Acta*, 2011, **56**, 6536.
- S5. See, for example, H. Rossotti, *Diverse Atoms: Profiles of the Chemical Elements*, Oxford University Press, Oxford, 1998.
- S6. See, for example, P. R. Roberge, *Corrosion Engineering: Principles and Practice*, McGraw Hill, New York, 2008.
- S7. C. Wagner, W. Traud, *Z. Elektrochem.*, 1938, **44**, 391.
- S8. I. B. Svir, A. V. Klimenko, R. G. Compton, *Radiotekhnika*, 2001, **118**, 92.
- S9. J. D. Wadhawan, *Electrochemical Sensor Engineering*, Oxford University, 2003.
- S10. A. C. West, T. F. Fuller, *J. Appl. Electrochem.*, 1996, **26**, 557.